33rd Annual International Conference of the IEEE EMBS
Boston, Massachusetts USA, August 30 - September 3, 2011

Manifold learning for shape guided segmentation of Cardiac boundaries: Application to 3D+t Cardiac MRI

Abouzar Eslami, Mehmet Yigitsoy, and Nassir Navab

Abstract. In this paper we propose a new method for shape guided segmentation of cardiac boundaries based on manifold learning of the shapes represented by the phase field approximation of the Mumford-Shah functional. A novel distance is defined to measure the similarity of shapes without requiring deformable registration. Cardiac motion is compensated and phases are mapped into one reference phase, that is the end of diastole, to avoid time warping and synchronization at all cardiac phases. Non-linear embedding of these 3D shapes extracts the manifold of the inter-subject variation of the heart shape to be used for guiding the segmentation for a new subject. For validation the method is applied to a comprehensive dataset of 3D+t cardiac Cine MRI from normal subjects and patients.

I. Introduction

Magnetic resonance imaging of the heart provides valuable information of its anatomy and functionality with high soft tissue contrast [1]. However, manual studies of the cardiac MRI sequences are usually tedious and time consuming and do not provide quantitative information that makes demands for automated and semi-automated approaches.

A wide variety of approaches for segmentation of cardiac boundaries are proposed in the literature. In [2], 4-D watershed was used. In [3], intensity- and texture-based fuzzy affinities are employed. Joint segmentation and motion estimation based on Mumford-Shah's functional and optical flow was applied to cardiac Cine MRI in [4]. Iterative thresholding and active contour with adaptation was proposed by Lee et al. [5]. A dual level set approach, coupled with data adherence term and myocardium incompressibility constraint was recently proposed by Zhu et al. [6].

Prior information of heart shape, appearance and deformation was utilized for segmentation of the heat chambers. A shape constrained deformable model with piecewise affine transform optimization was used in [7]. Andreopoulos et al. [8] proposed using 3-D active appearance model followed by 2-D+t active shape model. Lynch et al. [9] applied non-rigid parametric temporal model of ventricular wall's deformation. Zhang et al. [10] used a 4-D model for preliminary segmentation of left and right ventricles, followed by intra-frame process with a 3-D model.

Manuscript received on April 10th , 2011.

A. Eslami, M. Yigitsoy and N. Navab are with the Chair for Computer Aided Medical Procedures and Augmented Reality, Technical University of Munich, Germany. (phone: +49 (89) 289-19403; fax: +49 (89) 289-17059; e-mail: eslami@cs.tum.edu).

In this paper, we use manifold learning to find the lower dimensional embedding of the heart shapes that represents the inter-subject variation. We use this manifold to import shape prior information to the segmentation problem and make a guided segmentation based on the training data samples. Manifold learning is a non-linear dimensionality reduction technique based on the assumption that the data in the higher dimensional space has a small number of degrees of freedom and data points are lying on a low dimensional manifold [11]. Manifold learning is used for visualization and classification of morphometric difference [12]. In [13] it is used as a tool to model the breathing and cardiac functionality. Hamm et al. [14] proposed a framework for large deformation registration using the manifold structure of the data. Georg et al. [15] used learned manifold coordinates for 4D CT construction. Wachinger et al. [16] applied manifold learning to 4D ultrasound reconstruction. Etyngier et al. [17] learn shape prior manifold to guide the image segmentation.

In the first part of this paper we provide a framework for modeling the heart shape based on manifold learning with a new distance measure defined from the phase field approximation of the Mumford-Shah's functional. We prepare the 3D training data set by determining a region of interest and then compensating for the cardiac motion into a reference phase, i.e. end of diastole. Thus, for each subject in the training set, a set of shape samples at end diastole are created to obtain a dense collection of data points and a statistically more robust model. In this way, there is no need for synchronization between sequences. Having created a densely sampled shape space, we find a lower dimensional embedding of this dataset to be used for guiding the segmentation in the second part. In the second part of this paper we propose a shape guided approach for segmentation of cardiac boundaries based on the learned manifold. We validated our approach on a comprehensive database and provide quantitative results.

II. Methodology

Our framework of shape guided segmentation is founded on the phase field approximation [18] of the Mumford-shah functional [19] for representing the shape. The resulting high dimensional space of shape is then embedded to the lower dimensional manifold of admissible shapes which will guide segmentation of new sequences.

A. Phase field representation of shape

Mumford and Shah, in their pioneering work [19], propose a functional of the edge set (Γ) and smooth approximation (I) for segmentation of the input image $\mathcal{I}$ so that excluding the

edge set from the image domain (Ω) yields a smooth approximation of the input image. Later, Ambrosio and Tortorelli [18] proposed approximation to the Mumford-Shah functional, by defining phase field variable $\zeta: \Omega \to R$ to be negligible at edges and almost 1 elsewhere. Then the solution to the segmentation problem can be realized by iteratively solving the set of corresponding Euler-Lagrange equations:

$$I - \nabla \cdot \left(\frac{\mu}{\lambda}(\zeta^2 + k_\epsilon)\nabla I\right) = \mathcal{I} \tag{1}$$

$$\zeta\left(\frac{\mu}{2\epsilon\nu}|\nabla I|^2 + \frac{1}{4\epsilon^2}\right) - \Delta\zeta = \frac{1}{4\epsilon^2} \tag{2}$$

where $k_\epsilon = O(\epsilon) \ll 1$ is a small positive real value. The scale parameter ϵ controls the width of the extracted edge set represented, so a scaled representation of the shape is attained. Furthermore, the phase field representation of the shape is landmark free and continuous in $\mathcal{C}^1$ that allows us to define a new distance measure to be used for manifold learning. Hence, we define the shape of cardiac boundaries in the high dimensional space by the phase field representation and learn the corresponding manifold of these shape representations to guide segmentation of cardiac boundaries.

B. Manifold Learning

The general idea behind the manifold learning techniques is to find a low dimensional representation of data samples lying on a manifold in high dimensional space $\mathbb{R}^{\boldsymbol{N}}$ while preserving the local neighborhood. The problem is defined as finding the points $\boldsymbol{y_i} \in \boldsymbol{R^n}$ on the low dimensional manifold $\boldsymbol{\mathcal{M}}$, given a set of high dimensional points $\boldsymbol{x_i} \in \boldsymbol{R^N}$, $\boldsymbol{n} \ll \boldsymbol{N}$.

Sevaral manifold learning techniques have been proposed in the literature. Among them are Laplacian Eigenmaps [20], Isomap [21], and Diffusion Maps [22]. We employ Laplacian eigenmaps which is a spectral technique for non-linear embedding since it is well founded on mathematical concepts (Laplace Beltrami operator) and computationally efficient. Laplacian eigenmaps build upon the construction of a graph, which represents the neighborhood information of the data set. Subsequently, the graph Laplacian is applied to calculate a low-dimensional representation of the data that preserves the local neighborhood information in an optimal way**.** Each node on the graph represents one data point (phase field representation of cardiac boundaries in our case) and nodes are assigned weights depending on the k-nearest neighboring points. The embedding is then formulated as minimization of the low dimensional coordinates y_i:

$$E = \sum \left\|y_i - y_j\right\|^2 w_{ij} \tag{3}$$

where $w_{ij} = e^{-\frac{\mathfrak{D}(x_i, x_j)}{\gamma}}$, $\gamma > 0$ and $\mathfrak{D}(x_i, x_j)$ is the distance between each pair of data samples. Optimal solution can be achieved by solving the corresponding minimum eigenvalue decomposition problem.

C. Data embedding of heart shape

Various scenarios can be proposed for embedding of the 3D+t data of the shape, appearance and motion of heart. With respect to the shape of cardiac boundaries, there are two types of deformation: intra-subject deformation of heart along cardiac cycle and inter-subject deformation between individuals that is of more significance to be modeled.

The schematic diagram of the proposed framework for data embedding of the shape of cardiac boundaries is shown in Fig. 1. First we compensate for the heart motion for each subject by estimating the warping from the end of diastole to different cardiac phases to bring them into the reference time point of the end of diastole. Assume that $M_{k,0}$ is the estimated motion from end of diastole to the kth time point ($k \in 1, \cdots, K$) of the 3D+t volume sequence. By applying the inverse of the estimated motion $M_{k,0}^{-1}$ a set of 3D volumes $\left\{I_{[0]},\ I_{[1]} \circ M_{1,0}^{-1},\ \cdots\ ,\ I_{[K]} \circ M_{K,0}^{-1}\right\}$ at the reference phase is attained. By doing this, we avoid the need for time warping and synchronizing of the volume sequences at all phases.

After intensity normalization of the resulting set of volumes, the region of interest is determined by manually locating some points and applying the corresponding convex hull mask. Then we solve the set of Eq. (1) and Eq. (2) iteratively to attain the phase field representation of the shape of cardiac boundaries to be embedded.

Performance of manifold learning strongly depends on the distance measure for neighborhood selection and weighting. The conventional sum of squared difference (SSD) used in many applications does not appropriately imply distance of two images. A more appropriate but computationally complex measure can be defined by considering the warping between two images. We propose a new similarity measure based on the phase field representation of shape which has a better performance than SSD and does not need deformable registration of images. The distance is defined based on the Mumford-Shah's definition of the edge set and its phase field approximation.

$$\mathfrak{D}_\epsilon(\mathcal{I}_i, \mathcal{I}_j) = \int \left(\zeta_i^2 \left|\nabla I_j\right|^2 + |\nabla I_i|^2 \zeta_j^2\right) dx \tag{4}$$

Fig. 2 illustrates how the distance between two images $\mathcal{I}_i$ and $\mathcal{I}_j$ is measured based on the phase field representation of their edge sets ζ_i and ζ_j and their smooth version I_i and I_j in Eq. (4). Solid black lines represent three edge maps ($|\nabla I_1|, |\nabla I_2|, |\nabla I_3|$) that can be assumed to be one row of three images. The blue lines represent the phase field representation of the first edge map (ζ_1) corresponding to $|\nabla I_1|$. It can be seen how the overlay between $|\nabla I_2|$ and ζ_1 is different from the overlay between $|\nabla I_3|$ and ζ_1 when the scale parameter ϵ is large enough. Smaller values of the scale parameter provide more definite representation of the edge set and so the distance measure in Eq. (4). However, a too small scale value may eliminate the sensitivity to the distance of edges.

D. *Shape Guided Segmentation*

The learned manifold of heart shapes provides shape prior information that we use to guide segmentation of cardiac boundaries. Generalizing the Mumford-Shah functional to 3D+t, cardiac boundaries can be segmented by minimizing $E(\Gamma_{[0]},\cdots,\Gamma_{[K]},I_{[0]},\cdots,I_{[K]}) = \sum_{k=0}^{K} E(\Gamma_{[k]},I_{[k]})$ where

$$E(\Gamma_{[k]},I_{[k]}) \coloneqq \frac{\lambda}{2}\int_{\Omega}(I_{[k]}-\mathcal{I}_{[k]})^2 dx + \frac{\mu}{2}\int_{\Omega\setminus\Gamma_{[k]}}|\nabla I_{[k]}|^2 dx + \upsilon\,\mathcal{H}^{d-1}(\Gamma_{[k]}) \tag{5}$$

Applying the estimated cardiac motion $\mathcal{I}_{[k]} = \mathcal{I}_{[0]}\circ M_{k,0}$ we have:

$$E(\Gamma_{[0]},I_{[0]},\cdots,I_{[K]}) \coloneqq \sum_{k=0}^{K}\left(\frac{\lambda}{2}\int_{\Omega}(I_{[k]}-\mathcal{I}_{[k]})^2 dx + \frac{\mu}{2}\int_{\Omega\setminus\Gamma_{[0]}\circ M_{k,0}}|\nabla I_{[k]}|^2 dx\right) + \upsilon\mathcal{H}^{d-1}(\Gamma_{[0]}) \tag{6}$$

The estimated motion fields $M_{k,0}$ are assumed to be regularized so that $\mathcal{H}^{d-1}(\Gamma_{[0]}\circ M_{k,0})$ is limited if $\mathcal{H}^{d-1}(\Gamma_{[0]})$ is limited and so is excluded from the functional. Let ζ represent the edge set at the end diastole (Γ_0), then phase field approximation of the functional in Eq. (6) is

$$E(\zeta,I_{[0]},\cdots,I_{[K]}) \coloneqq \sum_{k=0}^{K}\int_{\Omega}\left(\frac{\lambda}{2}(I_{[k]}-\mathcal{I}_{[k]})^2 + \frac{\mu}{2}|\nabla I_{[k]}|^2(\zeta^2+k_\epsilon)\circ M_{k,0}\right)dx + \upsilon\int_{\Omega}\left(\epsilon|\nabla\zeta|^2+\frac{1}{4\epsilon}(1-\zeta)^2\right)dx \tag{7}$$

By using techniques of calculus of variation, the minimizer of the functional in Eq. (7) can be achieved by iteratively solving the set of Euler-Lagrange equations:

$$I_{[k]} - \nabla\cdot\left(\frac{\mu}{\lambda}(\zeta^2+k_\epsilon)\nabla I_{[k]}\right) = \mathcal{I}_{[k]} \tag{8}$$

$$\zeta\left(\frac{\mu}{2\epsilon\nu}\left(|\nabla I_{[0]}|^2 + \sum_{k=1}^{K} abs(|\mathrm{J}_{M_{k,0}}|)|\nabla I_{[k]}|^2\circ M_{k,0}^{-1}\right) + \frac{1}{4\epsilon^2}\right) - \Delta\zeta(x,t) = \frac{1}{4\epsilon^2} \tag{9}$$

In order to limit the space of feasible shapes to the learned manifold, we project the resulting ζ after each iteration to the lower dimensional manifold by the technique of out-of-sample extension proposed in [23]. Embedding for the new sample is computed as follows;

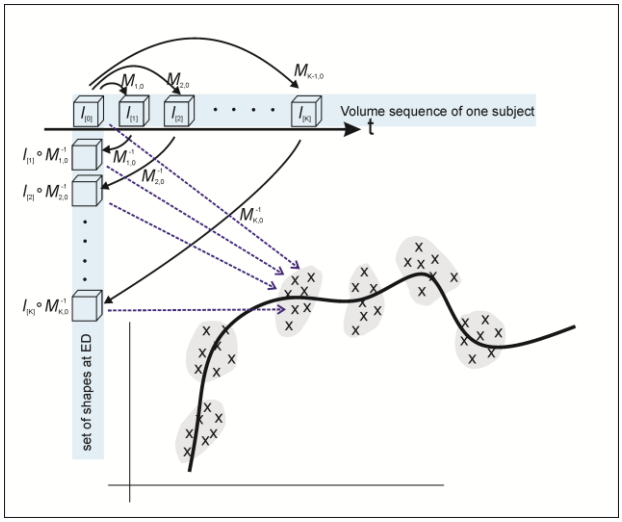

Fig. 1 Schematic diagram of the proposed shape embedding after compensation of cardiac motion.

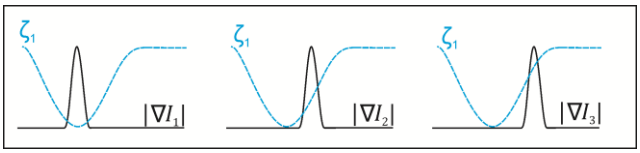

Fig 2. Demonstration of the defined distance measure in Eq. (4) based on the phase field representation of shape.

$$y'_m = \frac{\sqrt{n}}{\lambda_m}\sum_{i=1}^{p} v_{mi}\,w(x',x_i)\ ,\quad m = 1,2,\cdots n \tag{10}$$

where y' is the embedding for x'. It is basically adding a new row or column to the weight matrix of embedding and projecting it onto the space spanned by n eigenvectors computed previously. An illustration of the extension is shown in Fig. 3.

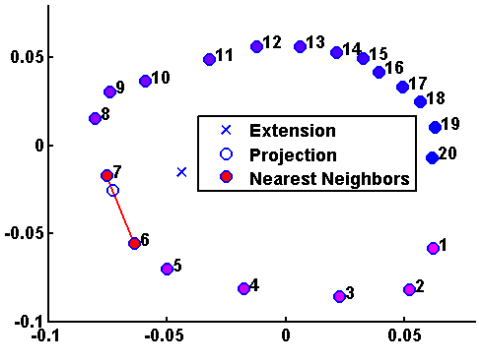

Fig. 3. Out-of-sample extension for embedding a new sample between samples 6 and 7.

We incorporate out-of-sample extension in the context of guided segmentation problem as follows:

- The already existing embedding is extended to the new data sample.
- The resulting embedding is projected onto the learned manifold of the training set.

- A new shape is constructed from the shapes corresponding to the nearest neighbors found after projection.
- The construction is done by interpolating a new shape $\zeta_{\mathcal{M}}$ using the deformation between the nearest shapes.
- The new shape is used to initialize the next iteration.

Finally, we propose our shape guided optimal solution based on the functional in Eq. (7) and the learned manifold of the heart shape:

Step 0 Compute the motion fields $M_{k,0}$ and initialize $I_{[k]} = \mathcal{I}_{[k]}$ for all k and $\zeta \equiv 1$

Step 1 Solve Eq. (8) for fixed ζ

Step 2 solve Eq. (9) for fixed $\{I_{[k]}\}$

Step 3 Find the corresponding shape $\zeta_{\mathcal{M}}$ on the learned manifold

Step 4 if ζ is not a stationary point then let $\zeta = \zeta_{\mathcal{M}}$ and go to step 1

III. Experimental Results and Discussion

The proposed method for shape guided segmentation is applied to a data set of 83 volume sequences. Images are taken from young (25), adult (43) and old (15) subjects with a wide range of heart shapes. Each sequence includes 20 frames of volumes by the size of $120 \times 120 \times 9$ after cropping into the region of interest. After motion compensation, a number of 1340 samples of the heart shape at end diastole are obtained from 67 subjects to be embedded. Phase field representation of the shape is then extracted from Eq. (1) and Eq. (2) for each sample to be embedded to the lower dimensional space, i.e. three dimensional shape prior manifold. Performance of the proposed distance measure in Eq. (4) can be seen in Fig. 4. The images in the right and the middle columns are the closest matches to the images in the left column with respect to the SSD and the defined distance, respectively. It can be seen in that the nearest images based on the defined distance measure are visually closer.

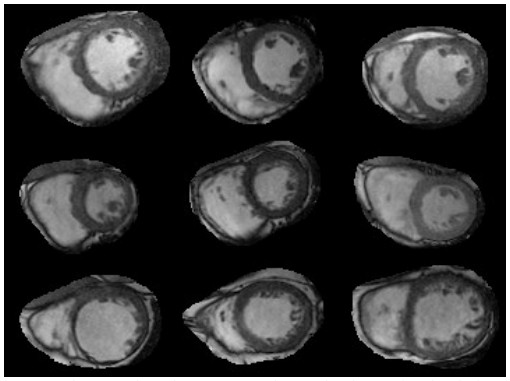

Fig. 4. In each row the closest sample to the heart in the left column with respect to the defined distance (middle) and the SSD (right) is shown.

Achievement of the proposed guided segmentation in segmenting weak and ambiguous boundaries is shown in Fig. 5. The proposed method is also quantitatively validated by computing the Dice metric ($\mathcal{D}$) [9] between the segmented object with a cardiologist's delineation. Table I reports the results of segmentation of the left ventricle's endocardium and epicardium and the right ventricle. Besides this technical metric, clinical measurements including end-diastolic volume (EDV), ejection fraction (EF) and left ventricle myocardium mass (MM) are computed and reported in table II. The Bland-Altman plot and the linear regression of the estimated values of EDV are shown in Fig. 6. Our experimental results support that the proposed shape guided segmentation algorithm is highly accurate and robust in segmenting the cardiac boundaries. The Bland-Altman analysis indicates that there is a good agreement between the results of the proposed shape guided segmentation and the manual segmentation. In addition, it does not need manual intervention except for determining the convex hull of the region of interest. However, the proposed approach is more successful in segmenting the left ventricle as the shape of the right ventricle has more variation than the left ventricle.

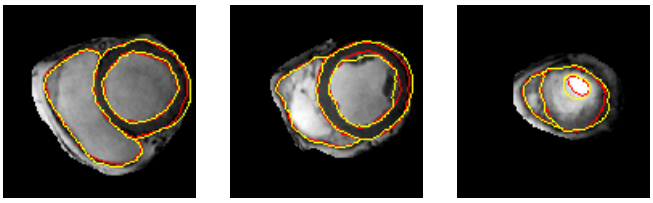

Fig. 5. Result of the proposed shape guided segmentation at three different slices

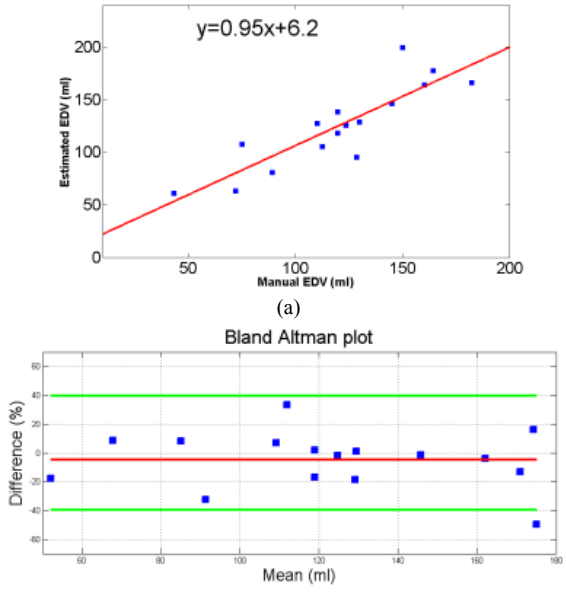

(a)

(b)

Fig.6. Resulted EDV in comparison with manual segmentation. (a) linear regression, (b) Bland-Altman plot.

The proposed framework for the shape modeling is non-linear learning of the shape prior manifold that in comparison with the linear PCA of active shape model represents the intra-subject variation more properly, especially when the variety increases in the studied population. Besides, much less effort is required for preparation of the training dataset as phase field

representation of the shape is used instead of landmark based shape representation and hence there is no need for manual segmentation of the training samples. The employed strategy of distributing the shape prior information from the end diastolic phase to other phases effectively avoided the need for temporal synchronization of the volume sequences at all cardiac phases. The proposed framework is in general applicable to the segmentation of other organs in other modalities as long as the phase field representation of the shape is not affected by the noise amount or very complex structure of the boundary.

Table I
Accuracy of the proposed method in Dice metric ($\mathcal{D}$%)

LV Endocardium	LV Epicardium	RV
93.83	89.25	91.40

Table II
Resulted clinical measurements from the proposed method in comparison with manual segmentation.

		EF (%)	MM (g)	EDV (mL)
Manual	$Ave \pm Std$	62.3 ± 14.2	109.5 ± 43.1	120.4 ± 36.9
Proposed	$Ave \pm Std$	60.8 ± 13.8	104.3 ± 48.8	125.3 ± 39.8
	$Corr$	0.86	0.81	0.88

IV. Conclusion

We proposed a framework for shape guided segmentation of cardiac boundaries based on the phase field representation of shapes and manifold learning without requiring time warping of the sequences and segmentation of training samples. We defined a new distance measure for manifold learning based on the phase field representation. Time warping of the sequences is avoided by taking the strategy of compensating the cardiac motion during training step and modeling the heart shape at the end of diastole and distributing the model to other cardiac phases during segmentation. The proposed method was applied to a comprehensive dataset including wide variety of heart shapes and its performance was compared to manual segmentation through technical and clinical measurements. Validation results illustrate benefits of our shape guided approach for segmentation of left and right ventricles.

References

[1] P. Kellman, C. Chefd'hotel, C. H. Lorenz, C. Mancini, A. E. Arai, E. R. McVeigh, "High Spatial and Temporal Resolution Cardiac Cine MRI from Retrospective Reconstruction of Data Acquired in Real Time Using Motion Correction and Resorting," Magnetic Resonance in Medicine, vol. 62, no. 6, p. 1557–1564, Sep. 2009.

[2] J. Cousty, L.Najman,M. Couprie, S.Clément-Guinaudeau, T.Goissen, J. Garot, "Automated, accurate and fast segmentation of 4-D cardiac MR images," Functional Imaging and Modeling of the Heart, vol. 4466, p. 474–483, 2007.

[3] U. Kurkure, A. Pednekar, R. Muthupillai, S.D. Flamm, I.A. Kakadiaris, "Localization and Segmentation of Left Ventricle in Cardiac Cine-MR Images ," IEEE Transactions on Biomedical Engineering, vol. 56, no. 5, pp. 1360 - 1370, 2009.

[4] A. Eslami, M. Jahed, T. Preusser, "Joint Denoising, Edge Detection and Motion Estimation of Cardiac MR Image Sequence by Phase Field Method," Computers in Biology and Medicine, vol. 40, no. 1, pp. 22-28, Jan. 2010.

[5] H.Y. Lee, N.C.F. Codella, M.D. Cham, J.W. Weinsaft, Y. Wang, "Automatic Left Ventricle Segmentation Using Iterative Thresholding and an Active Contour Model With Adaptation on Short-Axis Cardiac MRI," IEEE Trans. Biomed. Eng., vol. 57, no. 4, pp. 905-913, APRIL 2010.

[6] Y. Zhu, X. Papademetris, A.J. Sinusas, J.S. Duncan, "A coupled deformable model for tracking myocardial borders from real-time echocardiography using an incompressibility constraint," Medical image analysis, vol. 14, no. 3, pp. 429-448 , June 2010.

[7] O. Ecabert, J. Peters, H. Schramm, C. Lorenz, J. von Berg, M. J. Walker, M. Vembar, M. E. Olszewski, K. Subramanyan, G. Lavi, J. Weese, "Automatic model-based segmentation of the heart in CT," IEEE Trans. Med. Imag., vol. 27, no. 9, p. 1189–1201, Sep. 2008.

[8] A. Andreopoulos and J. K. Tsotsos, "Efficient and generalizable statistical models of shape and appearance for analysis of cardiac MRI," Med. Imag. Anal., vol. 12, no. 3, p. 335–357, Jun 2008.

[9] M. Lynch, O. Ghita, P.F. Whelan, "Segmentation of the Left Ventricle of the Heart in 3-D+t MRI Data Using an Optimized Nonrigid Temporal Model," IEEE Trans. Med. Imag., vol. 27, no. 2, pp. 195-203, Feb. 2008.

[10] H. Zhang, A. Whale, R. K. Johnson, T. D. Scholz, M. Sonka, "4-D cardiac MR image analysis: left and right ventricular morphology and function," IEEE trans. on Medical Imaging, vol. 29, no. 2, pp. 350-364, Feb. 2010.

[11] R. Pless, R. Souvenir, A Survey of Manifold Learning for Images, IPSJ Transactions on Computer Vision and Applications, Vol. 1, pp.83-94, 2009.

[12] R. Sparks, A. Madabhushi, Novel Morphometric Based Classification via Diffeomorphic Based Shape Representation Using Manifold Learning, Medical Image Computing and Computer-Assisted Intervention, Vol. 3, pp. 658-665, MICCAI 2010.

[13] Q. Zhang, R. Souvenir, R. Pless, On manifold structure of cardiac mri data: Application to segmentation, IEEE Conference on Computer Vision and Pattern Recognition, Vol. 1, pp. 1092-10698, 2006.

[14] J. Hamm, D.H. Ye, R. Verma, and C. Davatzikos, GRAM: A Framework for Geodesic Registration on Anatomical Manifolds, Medical Image Analysis, 2010.

[15] M. Georg, R. Souvenir, A. Hope, R. Pless, Simultaneous data volume reconstruction and pose estimation from slice samples, IEEE Conference on Computer Vision and Pattern Recognition, pp. 1-6, CVPR 2008.

[16] C. Wachinger, M. Yigitsoy, N. Navab, Manifold Learning for Image-Based Breathing Gating with Application to 4D Ultrasound, Medical Image Computing and Computer Assisted Intervention MICCAI 2010, pp. 26-33.

[17] P. Etyngier, F. Segonne, R. Keriven, Active-contour-based image segmentation using machine learning techniques, Medical Image Computing and Computer-Assisted Intervention, pp. 891-899, MICCAI 2007.

[18] L. Ambrosio, V. M. Tortorelli, "Approximation of Functionals Depending on Jumps by Elliptic Functionals Via Γ-Convergence," Comm. Pure Appl. Math., vol. 43, p. 999–1036, 1990.

[19] D. Mumford, J. Shah, "Optimal Approximation by Piecewise Smooth Functions and Associated Variational Problems," Comm. Pure Appl. Math., vol. 42, p. 577–685, 1989.

[20] M. Belkin, P. Niyogi, Laplacian eigenmaps for dimensionality reduction and data representation, Neural computation, Vol, 15, no. 6, pp. 1373-1396, 2003.

[21] J.B. Tenenbaum, V. Silva, J.C. Langford, A global geometric framework for nonlinear dimensionality reduction, Science, Vol. 290, no. 5500, pp. 2319, 2000.

[22] R.R. Coifman, S. Lafon, A.B. Lee, M. Maggioni, B. Nadler, F. Warner, S.W. Zucker, Geometric diffusions as a tool for harmonic analysis and structure definition of data: Diffusion maps, Proceedings of the National Academy of Sciences of the United States of America, Vol. 102, no. 21, pp.7426, 2005.

[23] Y. Bengio, J.F. Paiement, P. Vincent, O.Delalleau, N. Le Roux, M. Ouimet, Out-of-Sample Extensions for LLE, Isomap, MDS, Eigenmaps, and Spectral Clustering, proceedings of the 16 conference on Advances in neural information processing systems, pp. 177, 2004.